Barite mineralization in Kalana speleothems, Central Estonia: Sr, S and O isotope characterization

Mikk Gaškov[a], Holar Sepp[a], Tõnu Pani[b], Päärn Paiste[a] and Kalle Kirsimäe[a]

[a] Department of Geology, University of Tartu, Ravila 14A, 50411 Tartu, Estonia; mikk.gaskov@ut.ee
[b] Museum of Natural History, University of Tartu, Vanemuise 46, 51014 Tartu, Estonia

Abstract. Barite mineralization in association with calcitic speleothem precipitates in cave structures in Silurian Aeronian carbonate rocks in Kalana quarry, Central Estonia, was studied. Barite mineralization in Kalana occurs in two generations – euhedral bladed-tabular barite zonal crystals from a few to 10 cm in size, growing on the limestone-dolomite wall-rock (generation I), and sparsely placed thin tabular crystals a few millimetres thick and up to 1 cm in size, growing on calcitic crusts (generation II). The barite crystals of generation I are frequently found embedded by paragenetically later calcitic botryoidal crusts. The Sr and S isotopic composition of barite crystals shows a trend of increasing Sr isotope ratios (from 0.7114 to 0.7120) and $\delta^{34}S$ values (from 13‰ to 33‰) from the central parts towards the edges of zonal crystals. This suggests barite precipitation by mixing of two endmember fluids at varying ratios during barite formation: warm (up to 70 °C) reducing fluid bearing Ba, characterized by an elevated radiogenic Sr- and ^{34}S-enriched isotopic signal, and a cooler ambient fluid bearing an isotopically lighter dissolved sulphate, characterized by lower Sr isotope ratios. The excess of radiogenic ^{87}Sr in barite compared to Phanerozoic seawater values suggests Sr derived from a continental source, whereas sulphate was derived either from oxidized H_2S or a modified seawater source. Gradual increase in $\delta^{34}S$ values towards the outer zones could also indicate the ^{34}S enrichment due to bacterial sulphate reduction, even though there is no paired ^{34}S and ^{18}O enrichment of sulphate, characteristic of bacterial reworking. This can be interpreted as indicating an open system with limited sulphate resupply where the $\delta^{18}O$ composition of sulphate was equilibrated with warm ascending hydrothermal fluid.

Key words: hydrothermal, Sr isotopes, $\delta^{34}S$, $\delta^{18}O$.

INTRODUCTION

Barite ($BaSO_4$) is a widespread mineral in diverse geological settings including sedimentary and hydrothermal ones (Hanor 2000; Kontak et al. 2006; Griffith & Paytan 2012). It has a very low solubility and is typically undersaturated in natural waters (Rushdi et al. 2000). Barite precipitation can be initiated by a mixing of fluids carrying dissolved Ba and sulphate (Valenza et al. 2000; Greinert et al. 2002) by cooling of hydrothermal fluids (Pfaff et al. 2010) or by bacterial processes (Stevens et al. 2015). It can form massive, either sedimentary or hydrothermal deposits (Hanor 2000; Griffith & Paytan 2012), but is also common as a dispersed authigenic mineral in marine sediments (Paytan et al. 2002), in and around hydrothermal vents and cold methane seeps (Greinert et al. 2002; Torres et al. 2003), as a vein/gangue mineral typically in association with lead-zinc-fluorite mineralization (Magnall et al. 2016) and in cave deposits (Onac et al. 2007). The chemical–

isotopic composition of barite has been widely used as a robust palaeoenvironmental proxy of its depositional environments that enables us to decipher the origin of palaeofluids and to reconstruct the sulphur cycling-fractionation (Dymond et al. 1992; Paytan et al. 1996; Shen et al. 2001; Staude et al. 2011; Eickmann et al. 2014). Although barite is widespread globally, only few published reports are available on its occurrence in Estonian Palaeozoic rocks (e.g. Niin et al. 1981; Kiipli et al. 2004).

Recently, Eensaar et al. (2017b) reported botryoidal calcite speleothems associated with pyrite and abundant bladed-euhedral barite in small-scale fracture-controlled cave systems in Silurian Aeronian carbonate rocks exposed in Kalana quarry, Central Estonia. The isotope composition of calcite in these precipitates shows extreme depletion in ^{13}C and large variations in $\delta^{13}C_{PDB}$ values ranging from −11‰ to −56‰, which suggests a ^{13}C depleted carbon source for calcite precipitation, probably supplied by microbially mediated anaerobic

oxidation of methane (AOM) or other hydrocarbons. It is possible that these cave systems represent a unique setting of AOM and the precipitation of barite and botryoidal calcite in these caves was similar to that in methane-hydrocarbon seeps in the sea-floor, where barite and ^{13}C depleted calcite precipitation takes place at the sulphate–methane interfaces (Castellini et al. 2006). At these interfaces deep Ba- and methane-bearing fluids encounter shallow fluids/porewater that provides the sulphate for barite precipitation.

In this research the sulphur and Sr-isotope composition of barite mineralization associated with calcite speleothems in Kalana quarry was studied. The objective was to reveal the sources and evolution of the fluids responsible for barite mineralization and to understand the processes relevant to the formation of these unusual speleothem deposits.

GEOLOGICAL SETTING

Fracture and cave systems in Kalana quarry, Central Estonia (Fig. 1) occur in the carbonate rock succession of Aeronian (Llandovery, Silurian, ca 440 Ma) age, which in the local stratigraphical scheme belongs to the Raikküla Regional Stage (Tinn et al. 2009). The

Fig. 1. Schematic geological map of Estonia and location of Kalana quarry. 1, Ediacara; 2, Cambrian; 3, Ordovician; 4, Silurian; 5, Devonian. Modified after Eensaar et al. (2017a).

sequence is characterized by a series of shallowing-upward shelf carbonates deposited at or close to wave-base depths in the middle–upper part of the succession, indicated by cross-bedded carbonate grainstones and calcareous tempestite beds. The limestone exposed in the quarry is partly dolomitized and the whole section exposed in the quarry is cut by a series of sub-parallel and vertical to sub-vertical fractures and veins from a few to 10 cm wide, mostly in the southwest–northeast direction. The vein mineralogy is characterized by calcite, dolomite, pyrite and sphalerite-galena of low-temperature hydrothermal origin (Eensaar et al. 2017a). Some of the fracture zones are widened by karst and form small caves that stretch along the fractures (Eensaar et al. 2017b).

Small (up to 1 m wide, 15 m long and 1.5–2 m high) cave structures with speleothem precipitates, such as botryoidal calcite, spar calcite, barite crystal aggregates and pyrite, are mostly found in the central and southern part of the quarry in the sub-vertical contact zones between limestone and dolomite bodies. Barite, spar calcite and pyrite mineralization are also present in the narrower fractures/veins where botryoidal calcite speleothems are absent.

MATERIAL AND METHODS

The barite aggregates studied were collected from different cave systems and fractures/veins in different locations all over the quarry. Barite mineralization associated with botryoidal speleothem crusts was sampled in the southern and western parts of the quarry (Fig. 1), where a 0.5–0.7 m wide, 1.5 m high and approximately 10 m long cave-like structure was opened in 2009 (Eensaar et al. 2017b). The cave structure is not preserved because of the active mining in the quarry. The collection of different speleothem and wall rock samples is deposited and available at the Museum of Natural History and the Department of Geology, University of Tartu, collection No. 1690.

Macroscopic inspection, petrographic and analytical scanning electron microscopic (SEM) analysis and X-ray diffractometry (XRD) were performed to characterize mineral composition and paragenesis. The imaging and chemical analyses of polished aggregates were carried out with Zeiss EVO 15MA scanning electron microscope equipped with an Oxford X-MAX energy dispersive detector (EDS) system and AZTEC software for element analysis and distribution mapping. The XRD pattern analysis of speleothem and vein barite mineralization was carried out on the powdered unoriented preparations with the Bruker D8 Advance diffractometer using Johannson-type primary monochromator filtered Cu-$K\alpha$ radiation and the LyxEye detector system. Rietveld
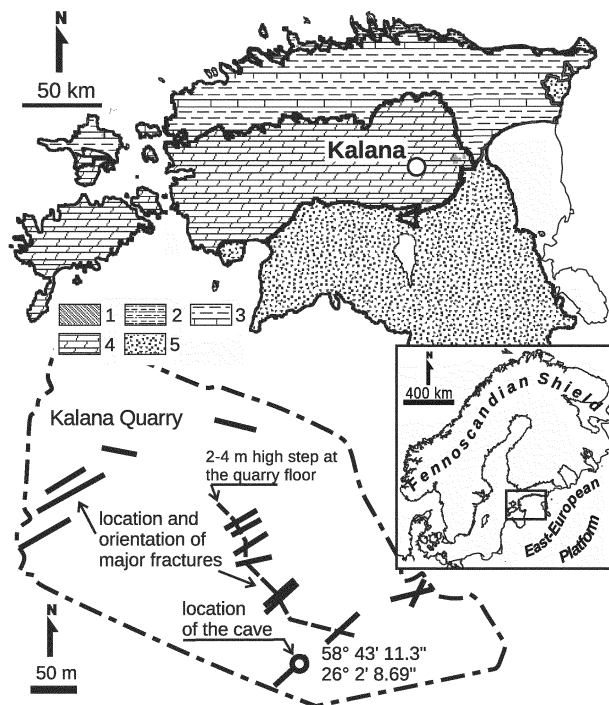
analysis of XRD patterns was carried out using the Siroquant 3.0 (Taylor 1991) code. X-ray fluorescence mapping of Sr in a polished barite aggregate slab was performed using a Rigaku Primus II spectrometer with a 1 mm spot size.

Sulphur isotope ratios (^{34}S/^{32}S) and oxygen isotope ratios (^{18}O/^{16}O) of pure $BaSO_4$ were analysed in powders microdrilled from handpicked and cleaned barite samples following a procedure described in Giesemann et al. (1994) and using a Thermo Finnigan Flash HT Plus elemental analyser interfaced to a Thermo Scientific Delta V Plus mass-spectrometer. The samples were calibrated to δ^{34}S and δ^{18}O values of NBS 127 and IAEA-SO-6. Sulphur isotope values are reported as relative to the Vienna Canyon Diablo Troilite (VCDT) in terms of a δ^{34}S$_{VCDT}$‰ and the sulphate oxygen isotope values are reported as relative to the Vienna Standard Mean Ocean Water (VSMOW) in terms of δ^{18}O. The long-term reproducibility of the barite δ^{34}S and δ^{18}O measurements was better than ±0.3‰.

The measurements of Sr isotope values of selected samples were carried out at the SGIker-Geochronology and Isotopic Geochemistry facility of the University of the Basque Country UPV/EHU (Spain). For these analyses approximately 100 mg of finely ground material was leached overnight in Teflon PFA vessels using 6N HCl at 100 °C. The solution was evaporated and the residue dissolved in 2.5 N HCl. Chemical procedures for sample treatment and Sr isolation followed those described in Pin & Bassin (1992). The ^{87}Sr/^{86}Sr ratios were measured using a high-resolution Thermo Fisher Scientific Neptune Multi Collector Inductively Coupled Plasma Mass Spectrometer (MC-ICP-MS) in static multicollection mode, and corrected for mass fractionation by normalization to ^{88}Sr/^{86}Sr = 8.375 209 (Steiger & Jäger 1977). The average ^{88}Sr/^{86}Sr ratio of NBS-987 standard over the period of analyses was 0.710 264 ± 0.000 006. The strontium content of Sr isotope samples was measured in the same powders dissolved in aqueous sodium carbonate according to Markovic et al. (2016) and analysed on Agilent 8800 ICP-MS.

RESULTS AND DISCUSSION

Petrography and chemical composition

The first generation of barite in the caves and veins of carbonate rocks in the Kalana sequence occurs as euhedral bladed-tabular (rhombic) barite crystals and crystal aggregates growing on the limestone-dolomite wall-rock (Fig. 2). On some occasions the barite aggregates show a macroscopically dendritic growth pattern (Fig. 2B). The size of the pale blue to transparent barite crystals of generation I reaches up to 7 cm in length, 5 cm in width

and up to 1–1.5 cm in thickness (Fig. 3A). Individual barite crystals cut along the long axis show zonal colouring typically from dark blue to pale blue/transparent and to dark blue (Fig. 3A). Under a polarizing microscope (Fig. 3B, C) the barite crystals show distinct growth bands that are few to tens of micrometres wide in the central parts of the crystal aggregates and grow wider (up to several millimetres in width) in the outer portions of the crystals. Growth bands are frequently decorated by abundant fluid inclusions, but a micro-thermometric analysis of these fluid inclusions for barite deposition temperatures was impossible to conduct, because most of the inclusions were single phase. The few two-phase inclusions were stretched/leaked upon heating.

The barite crystals growing in the fractures and the wall rocks are frequently encrusted with a 1–4 mm thick layer of microcrystalline pyrite aggregates (Fig. 2A). In the cave structures filled with botryoidal calcite speleothems the barite and pyrite successions are covered in curved-face columnar-bladed calcite aggregates that grade into a finely laminated calcite aggregate (Fig. 2A). In some cases barite has been intensely leached to white opaque microcrystalline calcitic masses. This leaching antedated the deposition of the botryoidal calcite in which the barite blades are embedded. The replacement of barite suggests varying oxidizing and reducing conditions as barite is readily destroyed in reducing environments (Hanor 2000). The second generation of barite occurs as sparsely placed thin (typically a few millimetres thick and up to 1 cm in width/length) pale-grey to white tabular crystals (Fig. 2C) on the surfaces of laminated botryoidal calcite aggregates, occurring in at least three repeated cycles (Eensaar et al. 2017b).

The morphology of barite crystals reflects the growth rates and is primarily dependent on the degree of supersaturation (Shikazono 1994). Euhedral, well-developed rhomboidal barite crystals characterize slow crystal growth rates at a low degree of supersaturation and are controlled by a surface reaction precipitation mechanism (Shikazono 1994). Dendritic growth patterns, however, are characteristic of precipitation from highly supersaturated solutions and are controlled by a diffusion-limited precipitation mechanism (Judat & Kind 2004). The dominant appearance of barite as tabular-bladed, well-developed crystal shapes and rare dendritic aggregates suggests slow precipitation rates at a low supersaturation level in Kalana. Barite precipitation experiments (Shikazono 1994) have shown that in laboratory conditions (temperature 150 °C, pressure equal to the vapour pressure of the aqueous solution) the well-developed crystals precipitate in solutions with the saturation index <20, whereas the formation of dendritic crystal aggregates required a saturation index of >20.
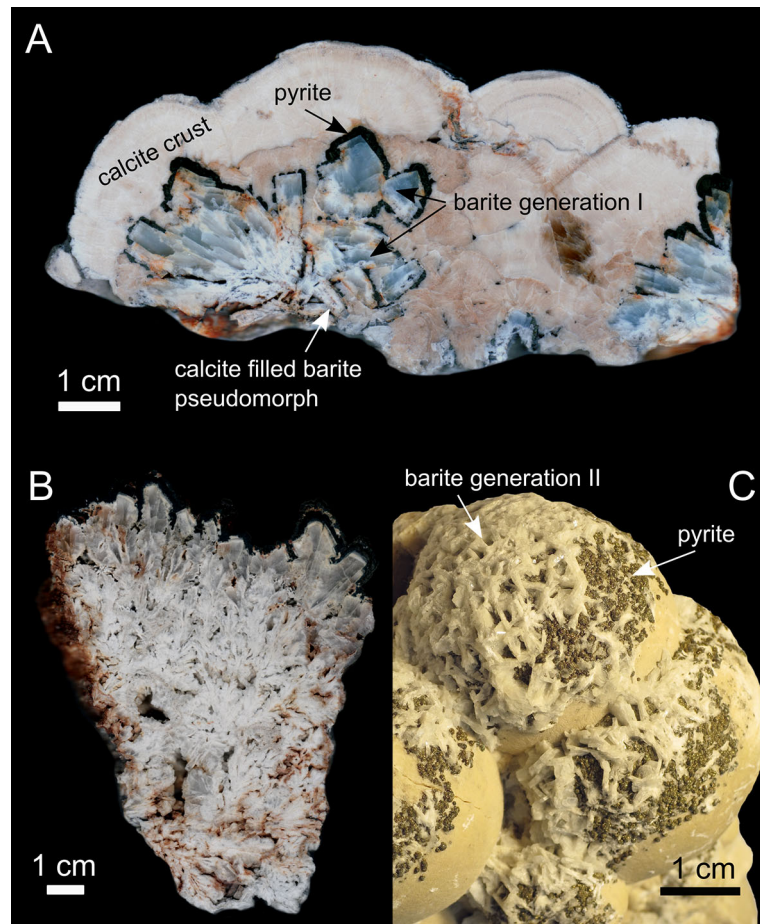
Fig. 2. Cross section of the botryoidal crust showing the cyclic character of barite–pyrite–calcite–barite–(pyrite) precipitation (**A**); cross section of dendritic barite aggregate (**B**) and barite generation II growing on calcite botryoidal aggregate (**C**).
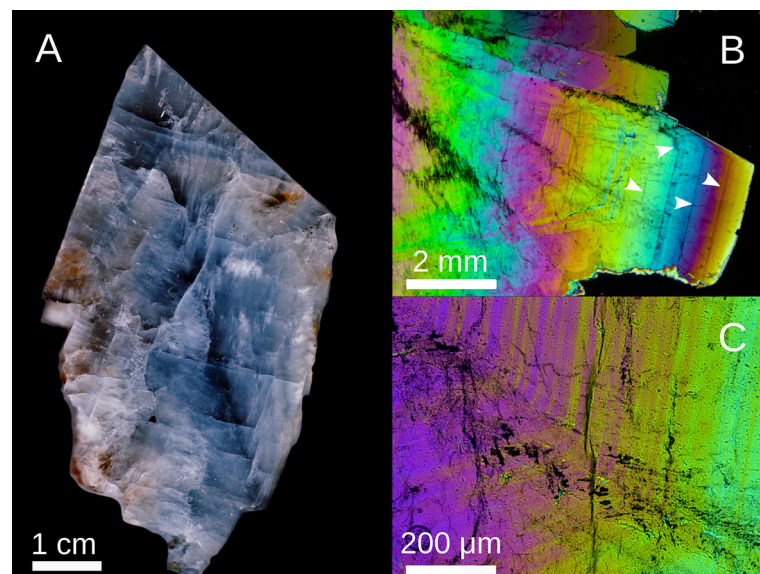
Fig. 3. Cross section of a tabular barite crystal showing macroscopic growth banding (**A**); microphotographs of growth bands under polarizing microscope in crossed polars, arrows indicate wider growth bands in outer parts of the crystal (**B**); fine growth bands in the central part of the zoned crystal (**C**).

The composition of barite is close to stoichiometric with little variation in unit cell parameters ($a = 8.865\,65 \pm 0.007\,63$ Å, $b = 5.450\,27 \pm 0.000\,62$ Å, $c = 7.147\,55 \pm 0.003\,71$ Å). The unit cell parameters suggest low $SrSO_4$ substitution in barite at Kalana (2–4 mol% $SrSO_4$ according to Goldish (1989). This is in accord with 0.1–1.6 wt% Sr measured in barite crystals (Table 1). However, the Sr content of barite crystals shows variation with respect to the growth zones and barite generations. Minute barite crystals of generation II are characterized by a Sr content typically less than 0.2 wt%. In the zonal crystals of generation I the central parts of the crystal aggregates show elevated Sr (up to 1.6 wt%), whereas Sr is progressively depleted in the outer zones of the larger crystals and the outermost growth zones have commonly Sr contents less than 0.3 wt% (Fig. 4A, B). The SEM microprobe analysis of the fine growth zones (Fig. 3B, C) within individual barite crystals indicates that Sr is higher in the darker zones and lower in bright zones.

The substitution of Sr in barite crystal structure is dependent on the crystallizing fluid, pressure, temperature and crystal growth rate. Barite precipitation experiments in conditions similar to that in seawater (Averyt & Paytan 2003) show that Sr partition increases with temperature. However, elevated Sr in hydrothermal barite can also be due to higher degrees of supersaturation and resultant faster crystal growth (Shikazono et al. 2012). Jamieson et al. (2016) have shown that in seafloor hydrothermal vent deposits the Sr substitution in barite does not show correlation with crystallization temperature, degrees of mixing between seawater providing sulphate and deep hydrothermal fluid carrying Ba, and fluid Sr concentrations, but is a function of crystal growth rate, whereas higher degrees of Sr substitution reflect periods of faster crystal growth driven by a higher degree of supersaturation. Higher Sr concentration in barite crystal aggregates in Kalana is characteristic of the central parts/zones of the aggregates

Table 1. Sulphur and oxygen isotopic composition, Sr isotope ratio and Sr concentration in the studied samples

| Sample	Generation	$\delta^{34}S_{VCTD}$ (‰)	$\delta^{18}O_{VSMOW}$ (‰)	$^{87}Sr/^{86}Sr$	Sr (wt%)
BAR-01-1	I	13.91	15.11	–	–
BAR-01-2	I	17.46	15.04	–	–
BAR-02-3	I	17.27	16.74	0.711\,563\,9	0.65
BAR-02-4	I	15.41	17.51	–	–
BAR-02-5	I	29.18	15.89	0.711\,930\,7	0.63
BAR-02-6	I	28.51	16.30	–	–
BAR-02-7	I	31.18	15.82	–	–
BAR-02-8	I	33.29	16.21	0.712\,032\,9	0.26
BAR-03-9	II	23.07	17.55	–	–
BAR-03-10	II	26.51	16.31	–	–
BAR-03-11	II	31.34	16.21	–	–
BAR-03-18	I	13.67	18.28	0.711\,410\,4	0.59
BAR-07-20	II	26.12	18.23	–	–
BAR-08-22	I	14.10	18.91	–	–
BAR-09-24	II	16.51	23.32	–	–
BAR-09-25	II	15.04	20.85	–	–
GB-01-30	I	14.13	17.59	–	–
GB-01-31	I	16.56	18.21	–	–
GB-02/03-34	I	25.88	15.33	–	–
GB-02/03-36	I	19.63	18.60	–	–
GB-10-37	I	13.40	16.68	–	–
GB-10-38	I	16.72	18.26	–	–
GB-06/07-41	I	23.04	16.64	–	–
GB-06/07-42	I	21.95	19.14	0.711\,548\,1	0.66
GB-06/07-43	I	30.46	17.41	0.711\,524\,2	0.46
GB-06/07-44	II	20.37	18.09	0.711\,589\,8	0.70
GB-04-45	I	19.57	17.82	0.711\,540\,6	1.50
GB-05-46	II	17.59	19.31	–	–

– not analysed.
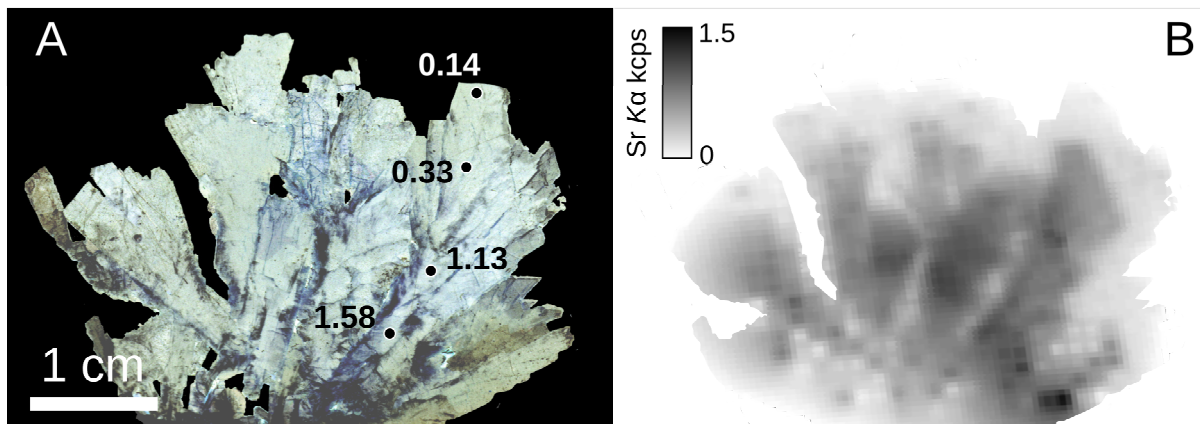
Fig. 4. Variation in Sr concentration (wt%) along a barite crystal aggregate of generation I according to EDS analyses (**A**); XRF mapping of Sr distribution in the same barite crystal aggregate, relative intensity of the Sr $K\alpha$ line, kcps – (kilo)counts per second (**B**).

and the Sr substitution rate decreases rapidly in the outer parts of the crystals, which suggests that over time the fluid became progressively less saturated with respect to barite in the Kalana fracture-cave systems. The first stages of barite crystallization were characterized by high growth rates under rapidly oscillating environmental conditions (possibly temperature) indicated by the fine zonation of barite crystal cores, whereas zones grow wider and show lower Sr concentration towards the outer faces of crystals, suggesting lower crystal growth rates under lower supersaturation conditions and possibly more stable environmental conditions.

Sr and S isotope composition

Barite whole-rock Sr isotope ($^{87}Sr/^{86}Sr$) ratios are reported in Table 1 and shown in Fig. 5. The Sr isotope ratios in the barite sampled in Kalana vary slightly from 0.711 410 to 0.712 033 and are very different from Palaeozoic values of 0.7077–0.7092 (McArthur et al. 2001) or modern seawater value of 0.709 183 (Butterfield et al. 2001). As long as there is no isotopic fractionation of Sr during barite precipitation, Sr derived from seawater or from the dissolution of normal marine carbonate host rocks would have a marine isotopic signature (Hanor 2000). However, the range of the enrichment of $^{87}Sr/^{86}Sr$
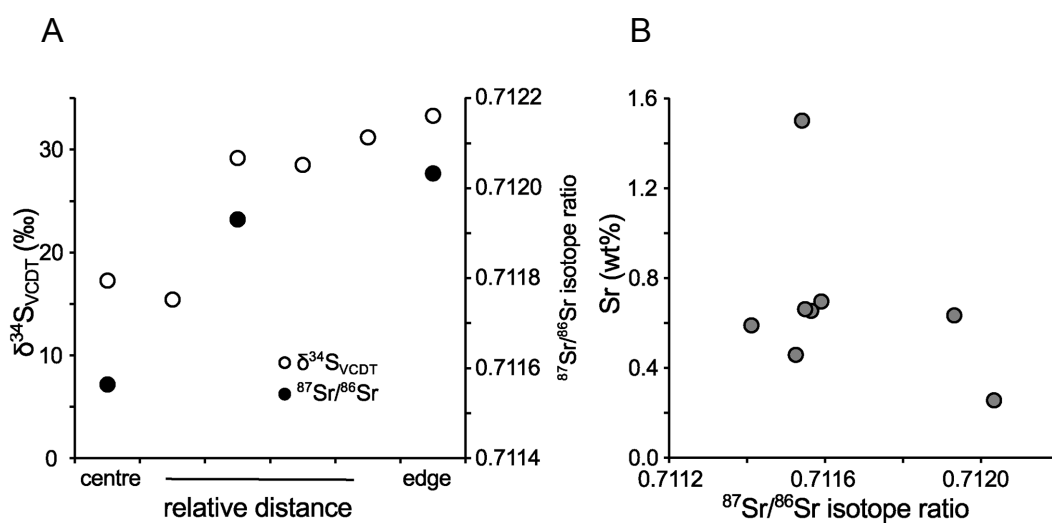
**Fig. 5.** Variation in Sr isotope ratios and sulphate $\delta^{34}S_{VCDT}$ values in a single crystal of generation I (**A**); cross-plot of $^{87}Sr/^{86}Sr$ ratios and Sr concentrations (**B**).

ratios (0.003–0.004) in comparison with seawater values contemporaneous or coeval with the depositional age of the host sediment is typical of Palaeozoic stratiform, and specifically of the cratonic hydrothermal barite deposits (Maynard et al. 1995). A similar discrepancy of barite and seawater isotopic compositions has also been observed in modern fluids discharging at cold seeps that have been interpreted to reflect the rock–water interaction of fluids before venting at the seafloor (Naehr et al. 2000; Torres et al. 2003). Therefore, we interpret the enrichment in Sr isotope ratios in Kalana barite to represent the excess radiogenic Sr derived from the alteration of silicates (e.g. K-feldspar) during the passage of the fluids in host rocks. This indicates that the barite in Kalana was not deposited (at least not directly) from seawater, but from evolved/deeper fluids. In large crystals with well-developed zonation the $^{87}Sr/^{86}Sr$ ratios show an increase outwards (Fig. 5A). However, there is no covariation between the Sr content and Sr isotope composition of the studied barite samples (Fig. 5B).

The S isotope composition of the studied barite samples ranges from 13‰ to 33‰ (Table 1, Fig. 6A). The $\delta^{34}S$ values of different barite generations overlap. The $\delta^{34}S$ values, however, show systematic variation in large, zonal barite crystals. The lowermost $\delta^{34}S$ values (<16‰) are found in the central parts of the crystals and the $\delta^{34}S$ values increase towards the edges, reaching up to 33‰ (Fig. 5B). The isotope composition of oxygen in barite varies typically between 15‰ and 19‰ and unlike the sulphur isotope composition, the sulphate $\delta^{18}O$ values do not show systematic variation with respect to the growth zones in larger crystals. Only a few barite

samples show ^{18}O-enriched composition with $\delta^{18}O$ values higher than 20‰.

Similarly to the Sr isotope ratios there is a negligible fractionation of sulphate S isotopes during the crystallization of sulphate minerals (ca 1.65‰). The $\delta^{34}S$ values of barite therefore represent the S isotope composition of dissolved sulphate in the barite-precipitating fluid (Seal et al. 2000). The $\delta^{34}S$ values of seawater-dissolved sulphate in the Phanerozoic varied from about 35‰ in the Cambrian–Ordovician, declined from 35‰ to 21.5‰ in the Silurian, dropped further down to about 18–20‰ for most of the Devonian and reached around 12–15‰ in the Carboniferous and Permian, finally trending back to about 20–22‰ about 45 million years ago (Paytan et al. 1998; Kampschulte & Strauss 2004; Algeo et al. 2015). The age of speleothem precipitation in Kalana is not known (Eensaar et al. 2017b), but if the seawater is considered as the reservoir providing sulphate, the large spread of the measured $\delta^{34}S$ values from 13‰ to 33‰ would be seemingly consistent with precipitation over a long time period from late Palaeozoic to Cenozoic. Nevertheless, barite formation over such a long time period is highly unlikely and the large variation in barite S isotope composition can instead be explained by bacterial sulphate reworking in a closed system through a Rayleigh-type fractionation process or in an open system with limited sulphate resupply (Canfield 2001). Bacterial consumption of sulphate (bacterial sulphate reduction – BSR) causes the ^{34}S isotope enrichment of the residual sulphate in the fluid and as a result the barite precipitating coevally with progressing BSR becomes isotopically enriched with respect to the heavy S isotopes
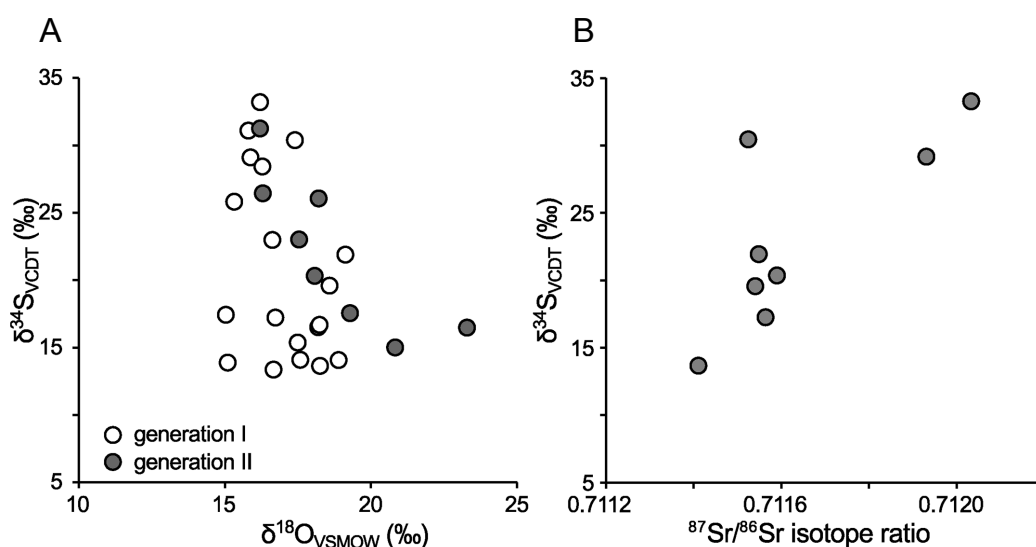
Fig. 6. Cross-plot of $\delta^{18}O_{VSMOW}$ and $\delta^{34}S_{VCDT}$ values in barite (**A**); cross-plot of measured $^{87}Sr/^{86}Sr$ ratios and sulphate $\delta^{34}S_{VCDT}$ values (**B**).

(Canfield 2001). The lowest $\delta^{34}S$ values (ca 13‰), found in the central parts of the barite crystals in Kalana, could then be considered to represent the composition of the initial dissolved sulphate, while the ^{34}S enrichment during crystal growth shows the evolution of the sulphate pool during BSR.

Seawater sulphate $\delta^{34}S$ values of comparable range (<15‰) were attained by the Carboniferous (ca 330 Ma) and were maintained through the Permian (Kampschulte & Strauss 2004), thus delimiting the age of barite precipitation. It is generally assumed that the Carboniferous–Permian seas did not reach the present-day Estonian territory and that the area has been higher than sea level since the late Devonian. However, the Carboniferous–Permian marine deposits occur in the erosional surface below the Quaternary glacial sediments in southwestern Latvia and Lithuania (Paškevičius 1997). The full extent of the sea during the Carboniferous and Permian in the Baltic basin is not known and it could be speculated that the Carboniferous and Permian seas bearing sulphate with low $\delta^{34}S$ values also invaded low-lying coastal areas about 200–300 km north of the area where these deposits are preserved in the present-day erosional surface. The long erosional period (<250 million years) since the end of the Permian would have effectively eroded away the Carboniferous–Permian deposits if any ever existed in the area under study. Interestingly enough, Liivrand (1990) has described redeposited Carboniferous spores in the Quaternary tills in southern Estonia and northern Latvia that would further support this hypothesis. The late Palaeozoic age of Kalana speleothem structures and mineralization is further supported by the fact that the carbonate rocks in Kalana bear a late Palaeozoic–Triassic overprinting on rock magnetization, possibly driven by a continental-scale fluid-flow event (Preeden et al. 2008).

Alternatively, the sulphate provided for barite crystallization could have originated from (a) direct dissolution of evaporites, (b) oxidation of sulphide minerals or (c) mineralization of organic matter. No evaporite deposits are known to exist in the rock sequences of the area where the Kalana cave systems are located. The occurrences of gypsum in the upper Devonian lagoonal evaporitic carbonate–claystone sequences in Latvia and northwestern Russia, right next to Estonia, show $\delta^{34}S$ values of >22‰ (Kalle Kirsimäe and Holar Sepp, pers. comm. 2016) and cannot be considered as the source of the sulphate. Sedimentary-diagenetic pyrite is a common accessory mineral in the Silurian carbonate rock sequences in Estonia with the $\delta^{34}S$ values in the lowermost Silurian rocks at about −20‰ (Hints et al. 2014). However, the sulphate produced by abiotic and/or biotic low-temperature oxidation of sulphide minerals

has $\delta^{34}S$ values of sulphate close to those of the source sulphides (Heidel et al. 2013), which would suggest a much more ^{34}S-depleted composition of the original sulphate compared to that measured in the barites with even the lowest $\delta^{34}S$ values.

On the other hand, the sulphur can be derived from the thermal degradation of organosulphur compounds, which results in H_2S with an isotopic composition that is close to (within 1–3‰) its parent organic matter/kerogen (Amrani et al. 2005). The sulphur isotopic composition of sedimentary organic matter depends on its origin and the maturation/sulphurization processes (Amrani 2014). As a result, the $\delta^{34}S$ values in the marine sedimentary organosulphur compounds can vary largely but are typically enriched in ^{34}S by up to 30‰ (on average 10‰) relative to co-existing pyrite (Anderson & Pratt 1995). Hypothetically, if the H_2S derived from the thermal maturation of this source is quantitatively oxidized into the sulphate through several intermediate species, including elemental sulphur, sulphite and thiosulphate (Zhang & Millero 1994), the dissolved sulphate would have an isotopic composition of up to ca 10‰. That is in the range of the lowest barite $\delta^{34}S$ values in Kalana. A similar oxidation process of (magmatically derived) H_2S and barite precipitation has been widely described in hydrothermal systems (Rye 2005).

Interestingly, there is a trend of increasing Sr isotope ratios and $\delta^{34}S$ values from the central/core parts of the large crystals towards the edges, whereas Sr isotope ratios and $\delta^{34}S$ values show positive covariation (Fig. 6B). Such covariation suggests a mixing of two endmember fluids at varying ratios – one being a more evolved fluid with elevated Sr isotope ratios and isotopically heavy sulphate, possibly derived from reworked porewater, and the other being a fluid bearing isotopically light sulphate and less radiogenic Sr isotope signature, possibly representing the original porewater (Maynard et al. 1995; Valenza et al. 2000). The mixing of two fluids bearing different isotopic signatures instead of a fractionation in a fully closed system is further supported by the range of the measured sulphate $\delta^{18}O$ values. In a closed system the Rayleigh-type fractionation in BSR also enriches the residual sulphate in ^{18}O (Aharon & Fu 2000). As a result, a linear correlation between $\delta^{18}O$ and $\delta^{34}S$ should be established in the residual sulphate pool. However, while the barite in Kalana has large variation of $\delta^{34}S$ values pointing to BSR, the $\delta^{18}O$ values are about 15‰ to 18‰ (in few cases >20‰; Fig. 6A), showing no enrichment in ^{18}O and thus implying that the fractionation process, if involving bacteria, did not proceed in a closed system, but rather in an open system with (limited) sulphate resupply. In this case the $\delta^{18}O$ values of sulphate are apparently equilibrated with the water

composition, meaning that the paired fractionation of sulphur and oxygen during BSR had minimal effect on oxygen isotopic composition.

Moreover, if the barite was crystallized under equilibrium conditions, fluid temperatures at the time of barite precipitation could be estimated using the isotope fractionation–temperature equation $10^3 \ln\alpha_{\text{mineral–water}} = 2.64 \, (10^6/T^2) - 5.3$ (Kusakabe & Robinson 1977). Assuming a fluid with the oxygen isotopic composition of Phanerozoic seawater –2‰ VSMOW (Veizer et al. 1999), the $\delta^{18}O$ values of barite mostly varying between 15‰ and 19‰ (median at 17.5‰) would indicate barite precipitation from a low-temperature hydrothermal fluid, with temperatures of ca 40–70 °C for generation I of barite and temperatures of ca 20 °C during the precipitation of generation II (Fig. 7). This range of temperatures agrees well with the fluid temperatures estimated for precipitation of ^{13}C-depleted calcite speleothem crusts succeeding the

first barite generation and preceding the second barite generation (Eensaar et al. 2017a). The $\delta^{18}O$ values of calcite crusts, increasing from –11‰ in the central parts of the botryoidal aggregates to –5‰ in the outer parts of the aggregates suggest the cooling of the low-temperature hydrothermal fluid from ca 70 °C to ambient temperature (Eensaar et al. 2017a).

CONCLUSIONS

We conclude that the barite in Kalana cave structures was deposited under varying oxidizing–reducing conditions as a result of the mixing of two fluids – a low-temperature (warm) reducing fluid bearing Ba, characterized by an elevated radiogenic Sr and ^{34}S enriched isotopic signal, and a cooler ambient fluid bearing isotopically lighter dissolved sulphate, characterized by lower Sr isotope ratios. The sulphate was derived either
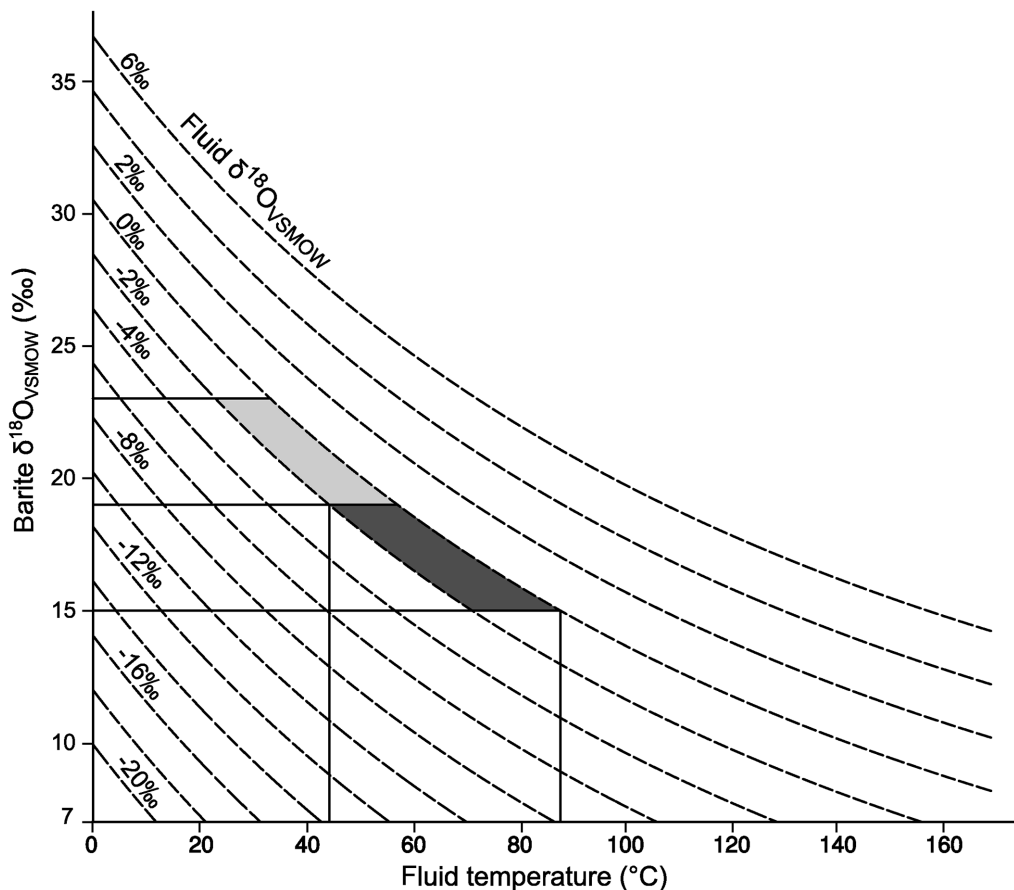
Fig. 7. Oxygen isotope fractionation curves for barite from the Kalana cave. Dark grey shading represents the spread of $\delta^{18}O_{\text{VSMOW}}$ in barite generation I and the light grey area shows variation in $\delta^{18}O_{\text{VSMOW}}$ values of barite generation II. Shaded areas illustrate the possible fluid temperatures assuming the Phanerozoic (sea)water with $\delta^{18}O_{\text{VSMOW}}$ values between –2‰ and 0‰ as the fluid source during barite precipitation.

from the oxidized H_2S developed by thermal maturation of buried sedimentary organic matter or from the seawater source, which in this case points to the Carboniferous–Permian seawater as the sulphate source and could delimit the age of barite precipitation. However, the $^{87}Sr/^{86}Sr$ values for barite range from 0.7114 to 0.7120, still reflecting a large contribution of radiogenic ^{87}Sr derived from a continental (but not leaching of marine carbonate) source. The gradual increase in $\delta^{34}S$ values towards the outer zones in the barite crystals in Kalana possibly indicates the presence of bacterial sulphate reduction that causes the ^{34}S isotope enrichment of the residual sulphate in the fluid, whereas the lack of the paired ^{34}S and ^{18}O enrichment, characteristic of bacterial reworking, indicates an open system with limited sulphate resupply where the $\delta^{18}O$ composition of sulphate was equilibrated with a warm ascending hydrothermal fluid. Seawater sulphate $\delta^{34}S$ values, the extent of Palaeozoic seas and carbonate rock remagnetization support the late Palaeozoic age of Kalana speleothem structures and mineralization.

REFERENCES

Aharon, P. & Fu, B. S. 2000. Microbial sulfate reduction rates and sulfur and oxygen isotope fractionations at oil and gas seeps in deepwater Gulf of Mexico. *Geochimica et Cosmochimica Acta*, **64**, 233–246.

Algeo, T. J., Luo, G. M., Song, H. Y., Lyons, T. W. & Canfield, D. E. 2015. Reconstruction of secular variation in seawater sulfate concentrations. *Biogeosciences*, **12**, 2131–2151.

Amrani, A. 2014. Organosulfur compounds: molecular and isotopic evolution from biota to oil and gas. *Annual Review of Earth and Planetary Sciences*, **42**, 733–768.

Amrani, A., Lewan, M. D. & Aizenshtat, Z. 2005. Stable sulfur isotope partitioning during simulated petroleum formation as determined by hydrous pyrolysis of Ghareb Limestone, Israel. *Geochimica et Cosmochimica Acta*, **69**, 5317–5331.

Anderson, T. F. & Pratt, L. M. 1995. Isotopic evidence for the origin of organic sulfur and elemental sulfur in marine sediments. *Geochemical Transformations of Sedimentary Sulfur*, **612**, 378–396.

Averyt, K. B. & Paytan, A. 2003. Empirical partition coefficients for Sr and Ca in marine barite: implications for reconstructing seawater Sr and Ca concentrations. *Geochemistry, Geophysics, Geosystems*, **4**(5), 1–14.

Butterfield, D. A., Nelson, B. K., Wheat, C. G., Mottl, M. J. & Roe, K. K. 2001. Evidence for basaltic Sr in midocean ridge-flank hydrothermal systems and implications for the global oceanic Sr isotope balance. *Geochimica et Cosmochimica Acta*, **65**, 4141–4153.

Canfield, D. E. 2001. Isotope fractionation by natural populations of sulfate-reducing bacteria. *Geochimica et Cosmochimica Acta*, **65**, 1117–1124.

Castellini, D. G., Dickens, G. R., Snyder, G. T. & Ruppel, C. D. 2006. Barium cycling in shallow sediment above active mud volcanoes in the Gulf of Mexico. *Chemical Geology*, **226**, 1–30.

Dymond, J., Suess, E. & Lyle, M. 1992. Barium in deep-sea sediment: a geochemical proxy for paleoproductivity. *Paleoceanography*, **7**, 163–181.

Eensaar, J., Gaškov, M., Pani, T., Sepp, H., Somelar, P. & Kirsimäe, K. 2017a. Hydrothermal fracture mineralization in the stable cratonic northern part of the Baltic Paleobasin: sphalerite fluid inclusion evidence. *GFF*, **139**, 52–62.

Eensaar, J., Pani, T., Gaškov, M., Sepp, H. & Kirsimäe, K. 2017b. Stable isotope composition of hypogenic speleothem calcite in Kalana (Estonia) as a record of microbial methanotrophy and fluid evolution. *Geological Magazine*, **154**, 57–67.

Eickmann, B., Thorseth, I. H., Peters, M., Strauss, H., Brocker, M. & Pedersen, R. B. 2014. Barite in hydrothermal environments as a recorder of subseafloor processes: a multiple-isotope study from the Loki's Castle vent field. *Geobiology*, **12**, 308–321.

Giesemann, A., Jager, H. J., Norman, A. L., Krouse, H. P. & Brand, W. A. 1994. Online sulfur-isotope determination using an elemental analyzer coupled to a mass-spectrometer. *Analytical Chemistry*, **66**, 2816–2819.

Goldish, E. 1989. X-ray diffraction analysis of barium-strontium sulfate (barite-celestite) solid solutions. *Powder Diffraction*, **4**, 214–216.

Greinert, J., Bollwerk, S. M., Derkachev, A., Bohrmann, G. & Suess, E. 2002. Massive barite deposits and carbonate mineralization in the Derugin Basin, Sea of Okhotsk: precipitation processes at cold seep sites. *Earth and Planetary Science Letters*, **203**, 165–180.

Griffith, E. M. & Paytan, A. 2012. Barite in the ocean – occurrence, geochemistry and palaeoceanographic applications. *Sedimentology*, **59**, 1817–1835.

Hanor, J. S. 2000. Barite–celestine geochemistry and environments of formation. In *Sulfate Minerals – Crystallography, Geochemistry and Environmental Significance* (Alpers, C. N., Jambor, J. L. & Nordstrom, K. D., eds), *Reviews in Mineralogy and Geochemistry*, **40**, 193–275.

Heidel, C., Tichomirowa, M. & Junghans, M. 2013. Oxygen and sulfur isotope investigations of the oxidation of sulfide mixtures containing pyrite, galena, and sphalerite. *Chemical Geology*, **342**, 29–43.

Hints, O., Martma, T., Männik, P., Nõlvak, J., Põldvere, A., Shen, Y. A. & Viira, V. 2014. New data on Ordovician stable isotope record and conodont biostratigraphy from the Viki reference drill core, Saaremaa Island, western Estonia. *GFF*, **136**, 100–104.

Jamieson, J. W., Hannington, M. D., Tivey, M. K., Hansteen, T., Williamson, N. M. B., Stewart, M., Fietzke, J., Butterfield, D., Frische, M., Allen, L., Cousens, B. & Langer, J. 2016. Precipitation and growth of barite within hydrothermal

vent deposits from the Endeavour Segment, Juan de Fuca Ridge. *Geochimica et Cosmochimica Acta*, **173**, 64–85.

Judat, B. & Kind, M. 2004. Morphology and internal structure of barium sulfate – derivation of a new growth mechanism. *Journal of Colloid and Interface Science*, **269**, 341–353.

Kampschulte, A. & Strauss, H. 2004. The sulfur isotopic evolution of Phanerozoic seawater based on the analysis of structurally substituted sulfate in carbonates. *Chemical Geology*, **204**, 255–286.

Kiipli, E., Kiipli, T. & Kallaste, T. 2004. Bioproductivity rise in the East Baltic epicontinental sea in the Aeronian (Early Silurian). *Palaeogeography, Palaeoclimatology, Palaeoecology*, **205**, 255–272.

Kontak, D. J., Kyser, K., Gize, A. & Marshall, D. 2006. Structurally controlled vein barite mineralization in the Maritimes Basin of eastern Canada: geologic setting, stable isotopes, and fluid inclusions. *Economic Geology*, **101**, 407–430.

Kusakabe, M. & Robinson, B. W. 1977. Oxygen and sulfur isotope equilibria in the $BaSO_4$–HSO_4–H_2O system from 110 to 350°C and applications. *Geochimica et Cosmochimica Acta*, **41**, 1033–1040.

Liivrand, E. 1990. *Methodical Problems of Pleistocene Palyno-stratigraphy*. Valgus, Tallinn, 176 pp.

Magnall, J. M., Gleeson, S. A., Stern, R. A., Newton, R. J., Poulton, S. W. & Paradis, S. 2016. Open system sulphate reduction in a diagenetic environment – isotopic analysis of barite ($\delta^{34}S$ and $\delta^{18}O$) and pyrite ($\delta^{34}S$) from the Tom and Jason Late Devonian Zn–Pb–Ba deposits, Selwyn Basin, Canada. *Geochimica et Cosmochimica Acta*, **180**, 146–163.

Markovic, S., Paytan, A., Li, H. & Wortmann, U. G. 2016. A revised seawater sulfate oxygen isotope record for the last 4 Myr. *Geochimica et Cosmochimica Acta*, **175**, 239–251.

Maynard, J. B., Morton, J., Valdes-Nodarse, E. L. & Diaz-Carmona, A. 1995. Sr isotopes of bedded barites: guide to distinguishing basins with Pb-Zn mineralization. *Economic Geology and the Bulletin of the Society of Economic Geologists*, **90**, 2058–2064.

McArthur, J. M., Howarth, R. J. & Bailey, T. R. 2001. Strontium isotope stratigraphy: LOWESS version 3: best fit to the marine Sr-isotope curve for 0–509 Ma and accompanying look-up table for deriving numerical age. *Journal of Geology*, **109**, 155–170.

Naehr, T. H., Stakes, D. S. & Moore, W. S. 2000. Mass wasting, ephemeral fluid flow, and barite deposition on the California continental margin. *Geology*, **28**, 315–318.

Niin, M., Niin, S., Puura, V. & Taalmann, V. 1981. Fissure fillings in limestone quarries around Tallinn. In *Settekivimid ja tektoonika* [*Sedimentary Rocks and Tectonics*] (Pirrus, E., ed.), pp. 113–125. Estonian Academy of Sciences, Tallinn [in Estonian].

Onac, B. P., Hess, J. W. & White, W. B. 2007. The relation-ship between the mineral composition of speleothems and mineralization of breccia pipes: evidence from Corkscrew Cave, Arizona, USA. *Canadian Mineralogist*, **45**, 1177–1188.

Paškevičius, J. 1997. *The Geology of the Baltic Republics*. Vilnius University, Geological Survey of Lithuania, Vilnius, 387 pp.

Paytan, A., Kastner, M. & Chavez, F. P. 1996. Glacial to interglacial fluctuations in productivity in the equatorial

Pacific as indicated by marine barite. *Science*, **274**, 1355–1357.

Paytan, A., Kastner, M., Campbell, D. & Thiemens, M. H. 1998. Sulfur isotopic composition of Cenozoic seawater sulfate. *Science*, **282**, 1459–1462.

Paytan, A., Mearon, S., Cobb, K. M. & Kastner, M. 2002. Origin of marine barite deposits: Sr and S isotope characterization. *Geology*, **30**, 747–750.

Pfaff, K., Hildebrandt, L. H., Leach, D. L., Jacob, D. E. & Markl, G. 2010. Formation of the Wiesloch Mississippi Valley-type Zn–Pb–Ag deposit in the extensional setting of the Upper Rhinegraben, SW Germany. *Mineralium Deposita*, **45**, 647–666.

Pin, C. & Bassin, C. 1992. Evaluation of a strontium-specific extraction chromatographic method for isotopic analysis in geological materials. *Analytica Chimica Acta*, **269**, 249–255.

Preeden, U., Plado, J., Mertanen, S. & Puura, V. 2008. Multiply remagnetized Silurian carbonate sequence in Estonia. *Estonian Journal of Earth Sciences*, **57**, 170–180.

Rushdi, A. I., McManus, J. & Collier, R. W. 2000. Marine barite and celestite saturation in seawater. *Marine Chemistry*, **69**, 19–31.

Rye, R. O. 2005. A review of the stable-isotope geochemistry of sulfate minerals in selected igneous environments and related hydrothermal systems. *Chemical Geology*, **215**, 5–36.

Seal, R. R., Alpers, C. N. & Rye, R. O. 2000. Stable isotope systematics of sulfate minerals. *Sulfate Minerals – Crystallography, Geochemistry and Environmental Significance*, **40**, 541–602.

Shen, Y. A., Buick, R. & Canfield, D. E. 2001. Isotopic evidence for microbial sulphate reduction in the early Archaean era. *Nature*, **410**, 77–81.

Shikazono, N. 1994. Precipitation mechanisms of barite in sulfate-sulfide deposits in back-arc basins. *Geochimica et Cosmochimica Acta*, **58**, 2203–2213.

Shikazono, N., Kawabe, H. & Ogawa, Y. 2012. Interpretation of mineral zoning in submarine hydrothermal ore deposits in terms of coupled fluid flow-precipitation kinetics model. *Resource Geology*, **62**, 352–368.

Staude, S., Gob, S., Pfaff, K., Strobele, F., Premo, W. R. & Markl, G. 2011. Deciphering fluid sources of hydrothermal systems: a combined Sr- and S-isotope study on barite (Schwarzwald, SW Germany). *Chemical Geology*, **286**, 1–20.

Steiger, R. H. & Jäger, E. 1977. Subcommission on geo-chronology: convention on the use of decay constants in geo- and cosmochronology. *Earth and Planetary Science Letters*, **36**, 359–362.

Stevens, E. W. N., Bailey, J. V., Flood, B. E., Jones, D. S., Gilhooly, W. P., Joye, S. B., Teske, A. & Mason, O. U. 2015. Barite encrustation of benthic sulfur-oxidizing bacteria at a marine cold seep. *Geobiology*, **13**, 588–603.

Taylor, J. C. 1991. Computer programs for standardless quantitative analysis of minerals using the full powder diffraction profile. *Powder Diffraction*, **6**, 2–9.

Tinn, O., Meidla, T., Ainsaar, L. & Pani, T. 2009. Thallophytic algal flora from a new Silurian Lagerstätte. *Estonian Journal of Earth Sciences*, **58**, 38–42.

Torres, M. E., Bohrmann, G., Dube, T. E. & Poole, F. G. 2003. Formation of modern and Paleozoic stratiform

barite at cold methane seeps on continental margins. *Geology*, **31**, 897–900.

Valenza, K., Moritz, R., Mouttaqi, A., Fontignie, D. & Sharp, Z. 2000. Vein and karst barite deposits in the western Jebilet of Morocco: fluid inclusion and isotope (S, O, Sr) evidence for regional fluid mixing related to central Atlantic rifting. *Economic Geology and the Bulletin of the Society of Economic Geologists*, **95**, 587–605.

Veizer, J., Ala, D., Azmy, K., Bruckschen, P., Buhl, D., Bruhn, F., Carden, G. A. F., Diener, A., Ebneth, S., Godderis, Y., Jasper, T., Korte, C., Pawellek, F., Podlaha, O. G. & Strauss, H. 1999. $^{87}Sr/^{86}Sr$, $\delta^{13}C$ and $\delta^{18}O$ evolution of Phanerozoic seawater. *Chemical Geology*, **161**, 59–88.

Zhang, J. Z. & Millero, F. J. 1994. Kinetics of oxidation of hydrogen-sulfide in natural-waters. *Environmental Geochemistry of Sulfide Oxidation*, **550**, 393–409.

Barüüdi mineralisatsioon Kalana speleoteemides: Sr, S ja O isotoopkoostised

Mikk Gaškov, Holar Sepp, Tõnu Pani, Päärn Paiste ja Kalle Kirsimäe

Töös uuriti Kalana karjääris (Kesk-Eesti) avatud Siluri Aeroni karbonaatkivimite läbilõikes leitud kaltsiitsete speleoteemidega kaasnevat barüüdi mineralisatsiooni ja selgitati barüüdi Sr, S ning O isotoopkoostist. Uuringu tulemused viitavad barüüdi tekkele kahe fluidi segunemisel. Üks neist oli arvatavasti hüdrotermaalne (kuni 70 °C) radiogeensest Sr ja ^{34}S poolest rikastunud redutseeriv Ba sisaldav, teine madalatemperatuuriline kergema isotoopkoostisega lahustunud sulfaati sisaldav fluid. Barüüdi väävliisotoopide koostise süstemaatiline rikastumine ^{34}S suhtes viitab sulfaadi bakteriaalsele ümbertöötlemisele sulfaadi suhtes suletud või piiratud süsteemis. Samas ei ole toimunud barüüdi sulfaadi rikastumist ^{18}O suhtes, mistõttu võib arvata, et tegemist oli süsteemiga, kus sulfaadi $\delta^{18}O$ väärtus tasakaalustus soojade tõusvate hüdrotermaalsete fluidide koostisega.